Menin determines K-RAS proliferative outputs in endocrine cells

Chester E. Chamberlain,[1,2,3] David W. Scheel,[1,2] Kathleen McGlynn,[4] Hail Kim,[1,2] Takeshi Miyatsuka,[1,2] Juehu Wang,[1,2] Vinh Nguyen,[5] Shuhong Zhao,[1,2] Anastasia Mavropoulos,[1,2] Aswin G. Abraham,[4] Eric O'Neill,[4] Gregory M. Ku,[2,6] Melanie H. Cobb,[4] Gail R. Martin,[3] and Michael S. German[1,2,6]

[1]Eli and Edythe Broad Center of Regeneration Medicine and Stem Cell Research, [2]Diabetes Center, and [3]Department of Anatomy, UCSF, San Francisco, California, USA. [4]CRUK/MRC Oxford Institute, Department of Oncology, University of Oxford, Oxford, United Kingdom. [5]Department of Surgery and [6]Department of Medicine, UCSF, San Francisco, California, USA.

Endocrine cell proliferation fluctuates dramatically in response to signals that communicate hormone demand. The genetic alterations that override these controls in endocrine tumors often are not associated with oncogenes common to other tumor types, suggesting that unique pathways govern endocrine proliferation. Within the pancreas, for example, activating mutations of the prototypical oncogene *KRAS* drive proliferation in all pancreatic ductal adenocarcimomas but are never found in pancreatic endocrine tumors. Therefore, we asked how cellular context impacts K-RAS signaling. We found that K-RAS paradoxically suppressed, rather than promoted, growth in pancreatic endocrine cells. Inhibition of proliferation by K-RAS depended on antiproliferative RAS effector RASSF1A and blockade of the RAS-activated proproliferative RAF/MAPK pathway by tumor suppressor menin. Consistent with this model, a glucagon-like peptide 1 (GLP1) agonist, which stimulates ERK1/2 phosphorylation, did not affect endocrine cell proliferation by itself, but synergistically enhanced proliferation when combined with a menin inhibitor. In contrast, inhibition of MAPK signaling created a synthetic lethal interaction in the setting of menin loss. These insights suggest potential strategies both for regenerating pancreatic β cells for people with diabetes and for targeting menin-sensitive endocrine tumors.

Introduction

K-RAS is a member of the RAS superfamily of membrane-bound GTPases that exist in either a GTP-bound active or GDP-bound inactive state (1). Signaling through G protein–coupled receptors and receptor tyrosine kinases can stimulate the formation of RAS-GTP, which then binds one of several downstream effectors to activate a signaling cascade. The best understood function for K-RAS is that of a mitogen and protooncogene working through the RAF/MAPK pathway to drive the expression of proproliferative genes in the nucleus. Activating mutants such as K-RAS^{G12D}, which block GTP hydrolysis and lock K-RAS in the activated state, act as dominant drivers of cellular proliferation and occur frequently in many types of cancer (Figure 1A and ref. 2).

However, K-RAS coordinates multiple, diverse, and sometimes opposing signaling networks (3), suggesting that K-RAS may have context-dependent functions. For example, expression of K-RAS^{G12D} stimulates transformation and tumor formation in pancreatic ducts and acini — but not in the pancreatic endocrine cells found in the islets of Langerhans, even after reducing the level of tumor suppressors *Cdkn2a* and *Trp53* (4). In addition, while *KRAS* is the most frequently mutated gene in pancreatic ductal adenocarcinoma (5), human pancreatic endocrine tumors never carry activating *KRAS* mutations (6).

▶ Related Commentary: p. 3698

Conflict of interest: The authors have declared that no conflict of interest exists.
Submitted: January 25, 2013; **Accepted:** June 26, 2014.
Reference information: *J Clin Invest*. 2014;124(9):4093–4101. doi:10.1172/JCI69004.

In contrast, pancreatic endocrine tumors more commonly inactivate tumor suppressors such as menin (6) or RASSF1A (7–9). RASSF1A, a product of the *RASSF1* gene, is an antiproliferative effector of activated K-RAS (10). Menin is the product of the *MEN1* gene. Heterozygous null mutations in *MEN1* cause multiple endocrine neoplasia type 1 (MEN1), an autosomal dominant cancer syndrome characterized by tumors of the endocrine cells of the pancreatic islets and the parathyroid and pituitary glands (11).

We hypothesized that the signaling networks downstream of K-RAS in pancreatic endocrine cells differed from those in K-RAS^{G12D}-sensitive cells such as the pancreatic acinar and duct cells. In testing this hypothesis, we discovered that mice heterozygous for a null mutation in *Kras* had increased numbers of pancreatic endocrine cells. Focusing on the insulin-producing β cells in the pancreatic islets, we found that their expansion came from 2 sources: increased production from neurogenin 3–expressing endocrine progenitors during embryogenesis and accelerated β cell proliferation during the perinatal period. In contrast, increased K-RAS signaling from constitutively active K-RAS^{G12D} suppressed both sources of new β cells, while still activating both the MAPK pathway and the RASSF1A pathway.

Kras heterozygosity also increased the proliferation of endocrine cells in 2 other tissues sensitive to *MEN1* mutation: the parathyroid and pituitary glands. In addition, we found that the dominance of the antiproliferative K-RAS effect in β cells depended on the expression of menin. Our data suggest a model in which K-RAS activates both the proproliferative MAPK pathway and the antiproliferative RASSF1A pathway. In the tissues

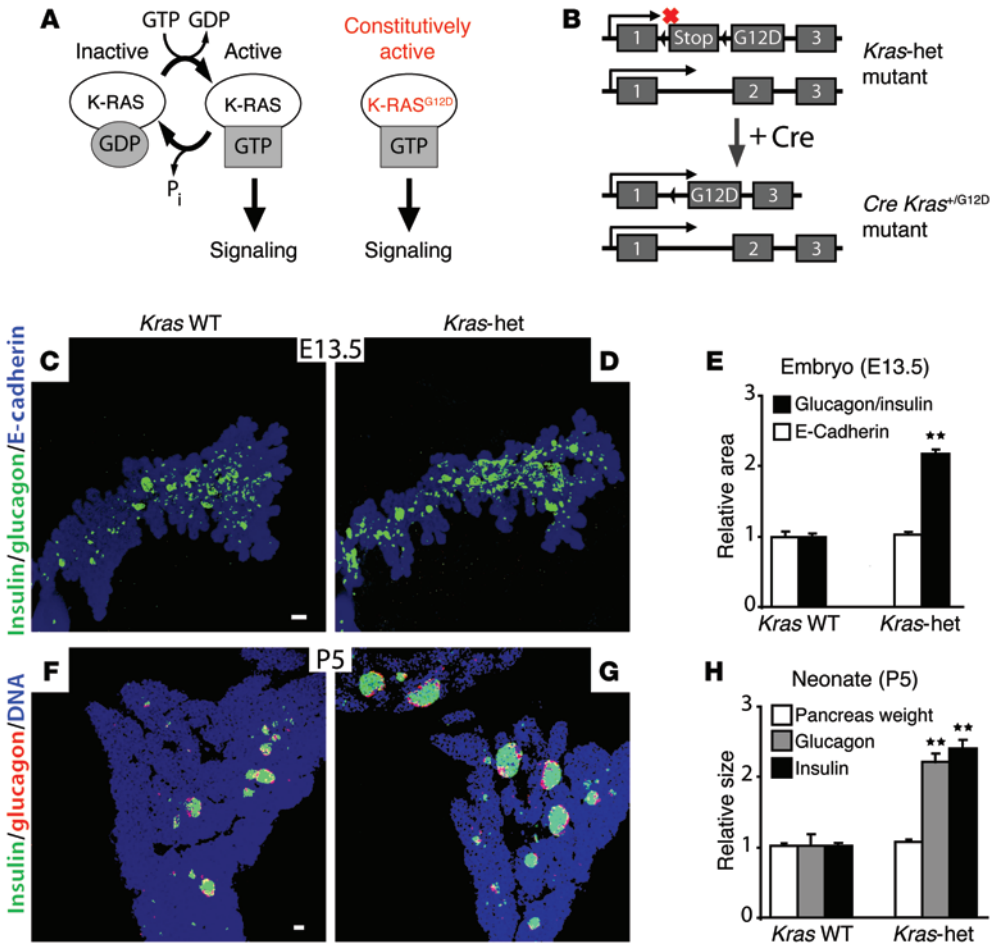

Figure 1. Pancreatic endocrine mass in *Kras*-het mice. (**A** and **B**) Schematic in **A** illustrates the relationship between K-RAS-GTP binding and intracellular signaling; schematic in **B** illustrates the conversion of the transcriptionally silent $Kras^{G12D}$–knock-in allele, which contains the G12D mutation in exon 2 and an upstream LoxP-Stop-LoxP sequence (12), to an active allele expressing constitutively active K-RAS^{G12D} after Cre-mediated recombination. (**C** and **D**) Projection images of the dorsal pancreas were collected by whole-mount confocal microscopy from E13.5 mouse embryos of the indicated genotypes and immunostained for E-cadherin (blue) and glucagon and insulin (green) (n = 6 *Kras* WT, n = 6 *Kras*-het). (**E**) Quantification of immunostained areas in the epithelial pancreas (E-cadherin) and endocrine pancreas (glucagon and insulin) relative to WT embryos. (**F**–**H**) Pancreatic sections from P5 WT (**F**) and *Kras*-het (**G**) neonates were immunostained for glucagon (red) and insulin (green), with quantification of the relative insulin and glucagon areas and pancreatic mass (**H**) (n = 3 *Kras* WT, n = 3 *Kras*-het). All data points represent the mean ± SEM. $^{**}P < 0.01$ versus WT animals by 2-tailed Student's t test. Scale bars: 50 μm.

susceptible to *MEN1* gene mutation, menin normally prevents the MAPK effector pathway from driving proliferation, while leaving inhibitory effector pathways such as RASSF1A intact. In this model, loss of menin causes proliferation in susceptible cells due to removal of the blockage of MAPK-driven proliferation downstream of K-RAS, while loss of K-RAS signaling increases proliferation by decreasing unopposed RASSF1A activity. Our data explain the absence of activating *KRAS* mutations and the high frequency of *MEN1* and *RASSF1A* inactivation in pancreatic endocrine tumors. Our study also suggests potential antiproliferative strategies for treating these tumors and proproliferative therapies for diseases that result from a deficiency of endocrine cell types, such as β cells, in both type 1 and type 2 diabetes.

Results

To test K-RAS function in pancreatic endocrine cell growth, we used mice carrying the $Kras^{G12D}$ allele, which is a null allele in the absence of Cre recombinase (12), in place of 1 WT allele (*Kras*-het; Figure 1B). We discovered that pancreata from E13.5 *Kras*-het embryos contained more endocrine cells, as determined by combined glucagon and insulin staining, than did WT pancreata, while overall pancreatic size remained unchanged (Figure 1, C–E, and Supplemental Figure 1; supplemental material available online with this article; doi:10.1172/JCI69004DS1). By P5, *Kras*-het animals had a relative expansion of both the glucagon-expressing α cell and insulin-expressing β cell populations without any increase in the exocrine pancreas (Figure 1, F–H, and Supplemental Figure 2). Further, *Kras*-het adults had improved glucose tolerance compared with that of WT controls (Supplemental Figure 3), consistent with an increase in functional β cell capacity.

Next, we sought to determine the source of additional endocrine cells in *Kras*-het animals. The fetal pancreas generates endocrine cells by neogenesis, followed by rapid expansion of those cells by proliferation during perinatal and postnatal growth (Figure 2A and ref. 13). Using expression of the transcription factor NEUROG3 to identify the transient precursor cells generated

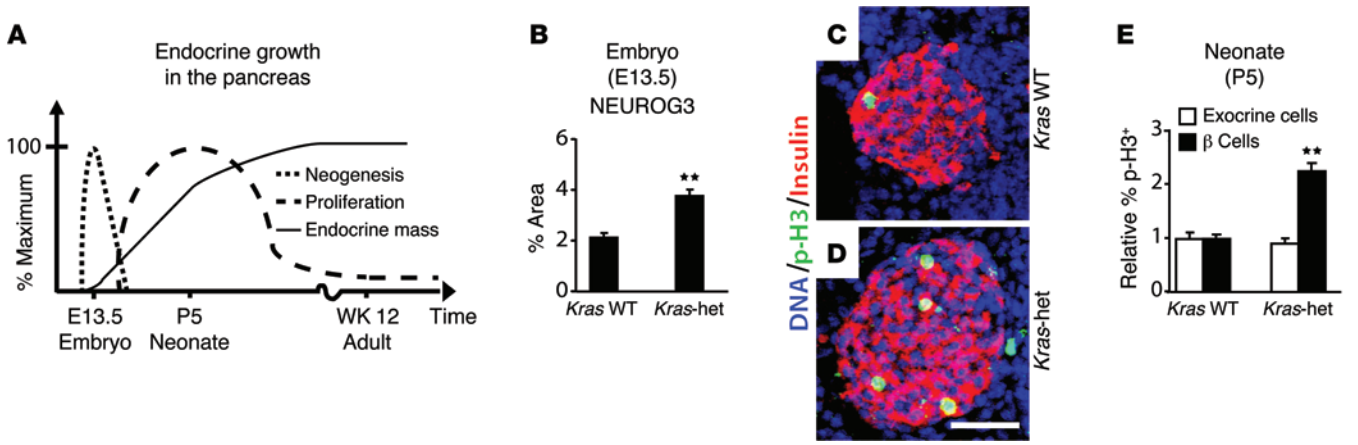

Figure 2. Endocrine neogenesis and proliferation in *Kras*-het mice. (**A**) Diagram shows the time course of endocrine neogenesis and proliferation in the mouse pancreas (13). (**B**) The percentage of the epithelial pancreas (E-cadherin) that immunostained for the endocrine neogenesis marker NEUROG3 was assessed in E13.5 mouse embryos of the indicated genotypes (n = 3 *Kras* WT, n = 3 *Kras*-het). (**C** and **D**) Pancreatic sections from P5 WT (**C**) and *Kras*-het (**D**) neonates were immunostained for insulin (red) and the proliferation marker p-H3 (green) and stained for nuclear DNA with DAPI (blue). (**E**) The percentages of β cells and exocrine cells that stained for the replication marker p-H3 are shown relative to those detected in WT embryos (n = 6 *Kras* WT, n = 6 *Kras*-het, >25,000 β cells and >50,000 exocrine cells were counted in total). All data points represent the mean ± SEM. $^{**}P < 0.01$ versus WT animals by 2-tailed Student's t test. Scale bar: 50 μm.

during endocrine neogenesis (14), we observed a marked increase in endocrine neogenesis in *Kras*-het pancreata at E13.5 (Figure 2B and Supplemental Figure 4). Staining with the proliferation marker phospho-histone H3 (p-H3) at this stage showed no endocrine cell proliferation in either *Kras*-het or WT controls (data not shown). At P5, however, during the postnatal period of endocrine proliferation, *Kras*-het β cells proliferated at twice the rate of those in WT controls, while exocrine cells showed no increase (Figure 2, C–E, and Supplemental Figures 5 and 6). Thus, loss of 1 *Kras* allele led to increases in both neogenesis and proliferation of endocrine cells in the pancreas.

To test the effect of increased K-RAS signaling, we used Cre recombinase to convert $Kras^{G12D}$ from a null allele into a gain-of-function allele that expresses constitutively active $K\text{-}RAS^{G12D}$ (Figure 1B) in pancreatic progenitor cells (*Pdx1-Cre*) or in β cells (*Ins2-Cre*) (Supplemental Figure 7). *Pdx1-Cre* $Kras^{+/G12D}$ embryos had no change in pancreatic size, but a marked reduction in the NEUROG3 expression field and in glucagon- and insulin-expressing cells (Figure 3, A–C). In *Ins2-Cre* $Kras^{+/G12D}$ pups at P5, we observed that β cells proliferated at markedly lower rates than was detected in *Ins2-Cre* control animals (Figure 3D and Supplemental Figure 8). These data demonstrate that K-RAS signaling directly antagonizes endocrine neogenesis in the embryo and proliferation in neonates.

Through distinct effectors, K-RAS can activate downstream pathways with opposing effects on cellular proliferation (3, 15). K-RAS effector B-RAF, which acquires activating mutations in many tumors, drives proliferation through activation of the MAPK pathway (2), while K-RAS effector RASSF1A blocks cell-cycle progression and is epigenetically silenced in many tumors (10). Pancreatic β cells express mRNA encoding multiple members of the RAS, RAF, and RASSF protein families (ref. 16 and Supplemental Figure 9). B-RAF and RASSF1 were broadly detected by immunostaining in the pancreas at P5, with relatively high expression in islets (Figure 3, E and F). To test the ability of K-RAS to activate these pathways in islets, we assayed for the phosphorylation of RASSF1 (Ser131) (p-RASSF1), which is critical for its tumor-suppressive activity (17), and ERK1/2 (Thr202/Tyr204) (p-ERK1/2), which lies downstream of B-RAF in the MAPK pathway (18), and detected an increase in the phosphorylated forms of both proteins broadly in β cells of *Ins2-Cre* $Kras^{G12D}$ mice as compared with the β cells of *Ins2-Cre* controls (Figure 3, G–J, and Supplemental Figure 10). We observed no changes in either p-ERK1/2 or p-RASSF1 in whole pancreas extracts from *Kras*-het animals (Supplemental Figure 10). However, p-RASSF1 was reduced in isolated *Kras*-het neonatal islets, while p-ERK1/2 remained unchanged (Supplemental Figure 10). Thus, K-RAS activates multiple downstream effector pathways in endocrine β cells, including those that have opposing effects on cellular proliferation.

Inhibition of K-RAS activity in cultured mouse or human pancreatic islets with a combination of farnesyl- and geranylgeranyl transferase inhibitors (FTI-GGTI) (ref. 19 and Supplemental Figure 11) yielded increased β cell proliferation (Figures 3, K–N, and Supplemental Figure 12). Treatment with the highly specific MEK1/2 inhibitor PD0325901 (20) had no effect on β cell proliferation (Figure 3M), even though ERK1/2 (Thr202/Tyr204) phosphorylation was blocked (Supplemental Figure 11). In contrast, we found that β cell proliferation in islets mutant for the "A" isoform of RASSF1 (*Rassf1a*) (21), which has antiproliferative activity (10), was increased and no longer sensitive to FTI-GGTI treatment (Figure 3M). These data indicate that K-RAS continues to suppress endocrine cell proliferation in the adult and that this activity depends on RASSF1A.

Heterozygous inactivating germline mutations of the *MEN1* tumor-suppressor gene that encodes menin cause multiple endocrine neoplasia type 1 (MEN1), an autosomal dominant cancer syndrome characterized by tumors in a subset of endocrine cell types, especially pancreatic islet, parathyroid, and pituitary (11). Similar to *Kras*-het mutants, reduced *Men1* gene dosage in mice

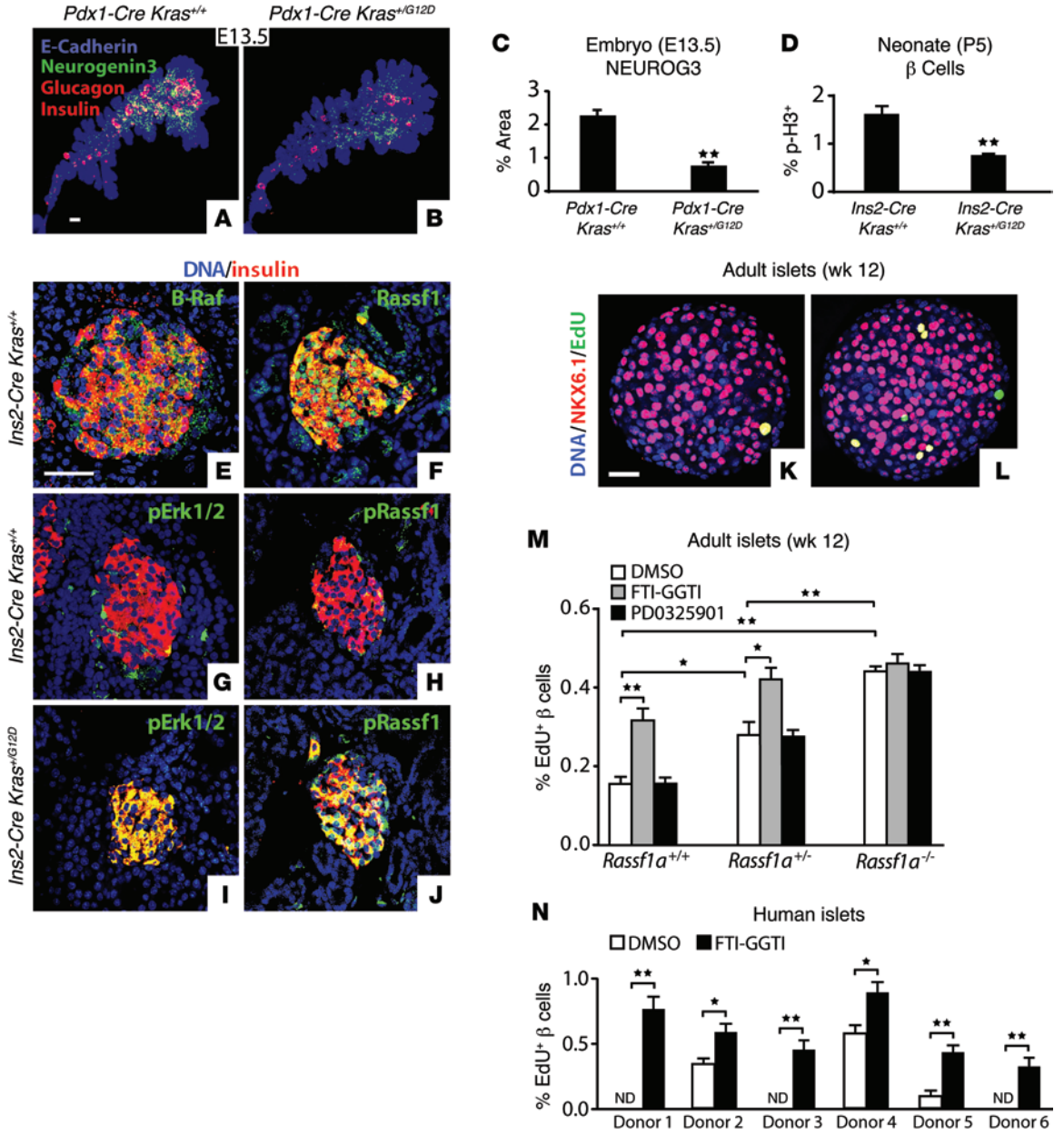

Figure 3. K-RAS signaling suppresses endocrine cell growth. (**A** and **B**) Projection images of the dorsal pancreas were collected by whole-mount confocal microscopy from E13.5 mouse embryos of the indicated genotypes and immunostained for E-cadherin (blue), NEUROG3 (green), and glucagon and insulin (red). (**C**) The percentage of epithelial pancreas that stained for NEUROG3 was quantified (n = 3 *Pdx1-Cre Kras*$^{+/+}$, n = 3 *Pdx1-Cre Kras*$^{+/G12D}$). (**D**) The percentage of β cells expressing the proliferation marker p-H3 was quantified in pancreata from P5 neonatal mice of the indicated genotypes (n = 5 *Ins2-Cre Kras*$^{+/+}$, n = 5 *Ins2-Cre Kras*$^{+/G12D}$, >25,000 β cells counted in total). (**E**–**J**) Sections from P5 neonatal pancreata of the indicated genotypes (n = 5 each) were immunostained for insulin, B-RAF, p-ERK1/2 (Thr202/Tyr204), RASSF1, and p-RASSF1 (Ser131). (**K**–**L**) Representative single optical sections from 12-week-old WT adult mouse islets treated with DMSO (**K**) or K-RAS inhibitor FTI-GGTI (**L**) that stained for β cell marker NKX6.1 (red), proliferation marker EdU (green), and nuclear DNA marker DAPI (blue). (**M** and **N**) The percentage of NKX6.1$^+$ β cell nuclei that costained for the proliferation marker EdU was quantified in islets from 12-week-old mice of the indicated genotypes (**M**, n = 3 replicates of >20 islets each, >430,000 β cells counted in total) or from human donors (**N**, 6 different donors, n = 3 replicates with >20 human islets each, >230,000 β cells counted in total) cultured with the additives shown and stained as in **K** and **L**. All data points represent the mean ± SEM. $^*P < 0.05$, $^{**}P < 0.01$ versus control by 2-tailed Student's t test. Scale bars: 50 μm. ND, none detected.

selectively increases islet cell growth and β cell proliferation as well as tumor formation in the MEN1 tissues, without affecting the exocrine pancreas or other cell types (22–24). We therefore examined whether other MEN1 tissues were affected in *Kras*-het mutants. We found that parathyroid glands were enlarged in *Kras*-het neonates relative to those in WT littermates (Figure 4, A and B, and Supplemental Figure 13), with increased proliferation of parathyroid chief cells, but not follicular cells, in the adjacent thyroid (Figure 4, C, D, and G, and Supplemental Figure 14). In the pituitary, we found that size and shape were unchanged (data not shown), but prolactin-expressing lactotrophs showed increased proliferation in *Kras*-het neonates relative to those in their WT littermates

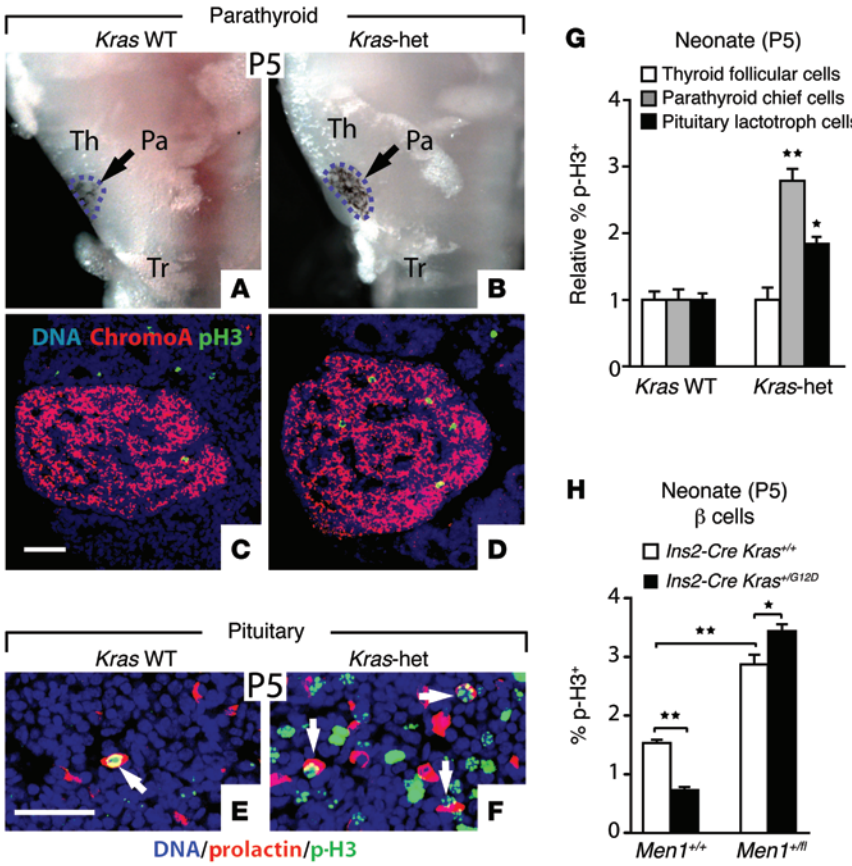

Figure 4. Endocrine proliferation in menin-sensitive tissues. (**A** and **B**) Ventral views of microdissected tissue from P5 neonates show the trachea (Tr), thyroid (Th), and parathyroid (Pa, outlined by intercalated black melanocytes). (**C** and **D**) Sections from P5 parathyroid glands were immunostained for the endocrine marker chromogranin A and p-H3. (**E** and **F**) Sections from P5 pituitary glands were immunostained for prolactin and p-H3. Proliferating lactotrophs are indicated with white arrows. (**G**) Normalized proliferation rates of the indicated cell types from P5 embryos were assessed by p-H3 staining (n = 6 *Kras* WT, n = 6 *Kras*-het, >6,000 chief cells, >3,000 lactotrophs, >14,000 thyroid follicular cells counted in total). (**H**) The percentage of β cells expressing the proliferation marker p-H3 was quantified in pancreata from P5 neonatal mice of the indicated genotypes (n = 4–5 for all genotypes, >34,000 β cells counted in total). All data points represent the mean ± SEM. $^*P < 0.05$, $^{**}P < 0.01$ versus control (**G**) or for the comparisons indicated by 2-tailed Student's t test. Scale bars: 50 μm.

(Figure 4, E–G, and Supplemental Figure 14). Thus, reduced *Kras* gene dosage increased the growth of endocrine cells in the pancreas, parathyroid, and pituitary. To test the interaction between K-RAS and menin, we used a conditional *Men1*-null allele (25). We found that reducing *Men1* gene dosage increased proliferation and switched K-RAS^{G12D} to an activator of proliferation in β cells of P5 neonates (Figure 4H), demonstrating that K-RAS function is dependent on menin in endocrine β cells.

It has been proposed that menin blocks growth by preventing p-ERK1/2 from driving cell-cycle progression (26). Consistent with this hypothesis, transgenic expression of menin in MIN6 insulinoma cells (Supplemental Figure 15) rendered the proliferation of these cells insensitive to the highly specific MEK1/2 inhibitor PD0325901 (20), which blocked ERK1/2 phosphorylation (Supplemental Figure 15). Conversely, we found that PD0325901 rescued the hyperproliferation of β cells with reduced *Men1* gene dosage (Figure 5, A–G). ERK1/2 phosphorylation was unaffected in *Ins2-Cre Men1*$^{+/fl}$ islets (Supplemental Figure 11). Remarkably, complete loss of *Men1* resulted in a synthetic lethal interaction (27) with PD0325901 (Figure 5F) or GSK1120212, another highly specific MEK1/2 inhibitor (data not shown) (28). Also, while FTI-GGTI elevates proliferation of adult WT and *Ins2-Cre* β cells, this effect was reversed in *Men1* mutant β cells (Figure 5G). Together, these data demonstrate that menin functions to block MAPK-driven proliferation in endocrine β cells.

Our data suggest a model in which menin determines K-RAS effects on endocrine cell proliferation by blocking proliferation driven by the MAPK pathway, while leaving K-RAS inhibitory pathways, such as RASSF1A, intact (Figure 5J). In this model, reduced menin gene dosage increases endocrine cell growth due to a reduction in blockage of MAPK-driven proliferation downstream of K-RAS, while reducing K-RAS gene dosage in endocrine cells with normal menin activity increases growth by decreasing the activity of the antiproliferative RAS effector RASSF1A. This model predicts that reduced menin activity might permit activators of the MAPK pathway to increase β cell proliferation. As predicted, the glucagon-like peptide 1 (GLP1) agonist exendin-4, which stimulates ERK1/2 phosphorylation in β cells (29), did not affect human β cell proliferation when added alone, but synergistically enhanced proliferation when combined with MI-2, an inhibitor of the interaction between menin and the histone methyltransferase MLL (ref. 30 and Figure 5, H and I).

Discussion

Despite its dominant role in stimulating growth in the exocrine pancreas (5), our data reveal that K-RAS acts to suppress growth in the pancreatic endocrine cells of the islets of Langerhans. This dichotomy further demonstrates how the same signaling pathway can generate opposing outputs in different cells (1–3, 31, 32) and provides an explanation for the divergent role of *KRAS* in the transformation of these 2 major pancreatic cell types (4–7, 33). The antiproliferative activity of K-RAS required the RAS effector RASSF1A, suggesting that *RASSF1A* silencing in pancreatic endocrine tumors (7, 9, 34–36) represents a release from the physiological growth inhibition imposed by this pathway. RASSF1A can inhibit cell proliferation by controlling the transcription of cell-cycle genes, the stability of cell-cycle proteins, or the stability of

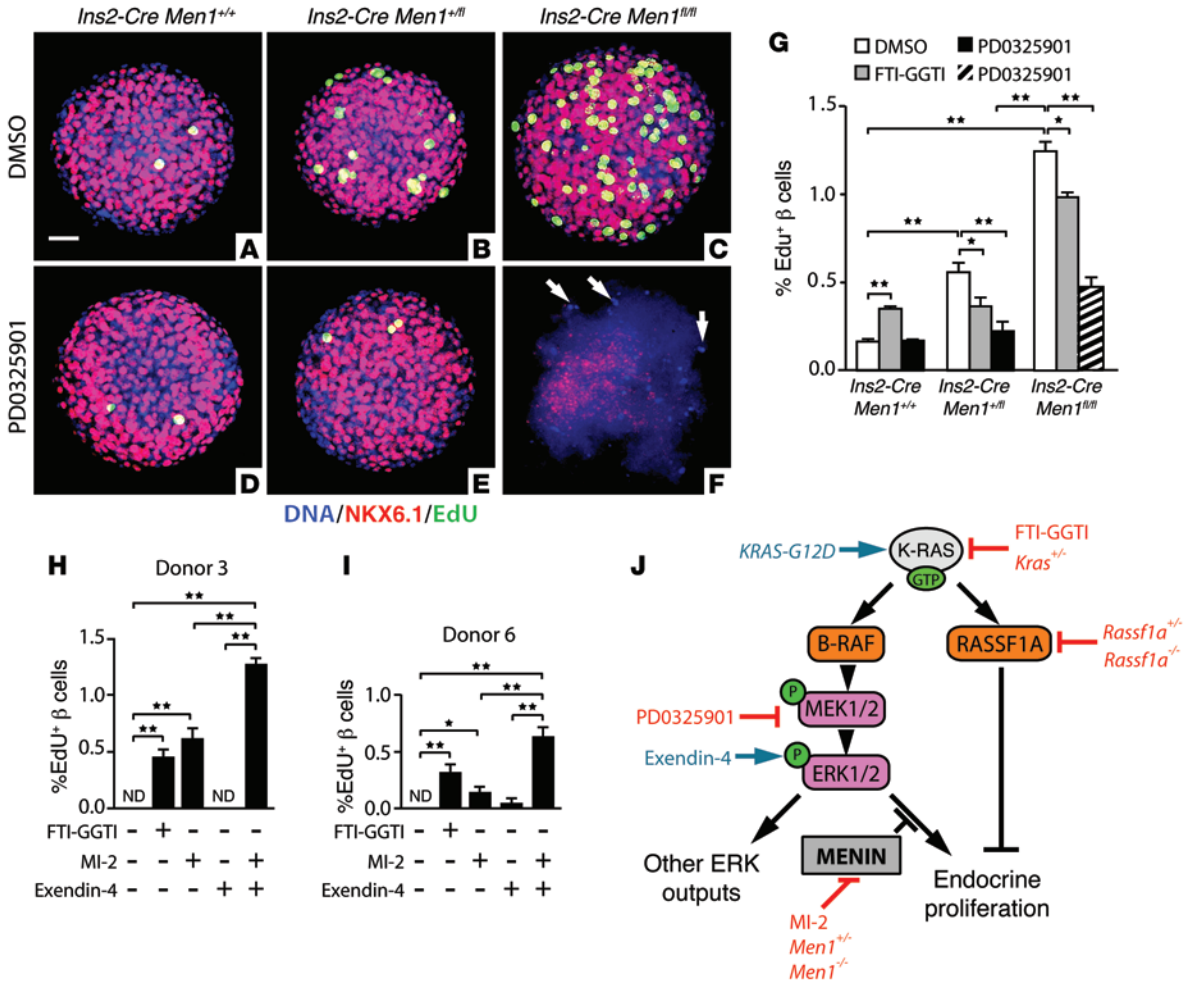

Figure 5. Control of MAPK-driven proliferation by menin determines K-RAS output in endocrine cells. (**A**–**F**) Projection images from whole-mount confocal microscopy of *Ins2-Cre Men1*$^{+/+}$ control, *Ins2-Cre Men1*$^{+/fl}$, and *Ins2-Cre Men1*$^{fl/fl}$ cultured mouse pancreatic islets (12-week-old males) immunostained for β cell marker NKX6.1 (red), proliferation marker EdU (green), and nuclear DNA marker DAPI (blue). Treatments and genotypes are indicated. In the islet shown in **F**, only NKX6.1$^-$ cells remained intact and stained for DAPI. In **G**, islets from 12-week-old mice of the indicated genotypes were cultured with the additives shown and stained as in **A**–**F**. Each bar represents the mean percentage of NKX6.1$^+$ β cell nuclei that costained for the proliferation marker EdU (n = 3 replicates of >20 islets for each condition, >480,000 β cells counted in total). Because β cells were completely destroyed by PD0325901 treatment in more than 70% of *Ins2-Cre Men1*$^{fl/fl}$ islets (**F**), only surviving β cells were used for quantification in this condition. In **H** and **I**, the same method was used to count the percentage of proliferating cells in human islets cultured with the indicated additives. Three repeats with more than 20 human islets each were performed for each donor; more than 185,000 β cells were counted. (**J**) Proposed model outlines the roles of menin and RASSF1A in modulating the control of proliferation by K-RAS function. All data points represent the mean ± SEM. $^*P < 0.05$, $^{**}P < 0.01$ for the comparisons indicated by 2-tailed Student's t test. Scale bar: 50 μm. ND, none detected.

microtubules (37–43). RASSF1A may also cooperate with other RASSF members to effect its action downstream of K-RAS (44).

In addition to the pancreas, endocrine tumors that arise from the parathyroids or pituitary are devoid of activating *KRAS* mutations (45–48) and frequently experience *RASSF1A* gene silencing (49, 50). Together with the endocrine pancreas, these tissues comprise the most common sites of tumorigenesis in people who inherit a single inactivating mutation in the menin-expressing *MEN1* gene (11, 51). Given the wide expression of K-RAS, RASSF1A, and menin, what mediates the cell specificity of tumor formation in people carrying *MEN1* gene mutations? We hypothesize that discrete cell types use distinct regulatory networks to specify and restrict the biological actions of K-RAS. In *MEN1*-sensitive endocrine cells, K-RAS activates opposing growth pathways, but antiproliferative pathways dominate due to the activity of menin, which prevents the MAPK pathway from driving growth, while leaving the inhibitory RASSF1A pathway intact. In this model, loss of menin increases proliferation due to removal of the blockage of MAPK-driven proliferation downstream of K-RAS, while loss of K-RAS signaling increases proliferation by decreasing unopposed RASSF1A activity (Figure 5J). The importance of the RAF/MEK/ERK pathway in driving the inappropriate growth and survival of endocrine cells with reduced menin activity offers a rationale for using inhibitors of this pathway for antiproliferative and cytotoxic therapy for tumors resulting from germline or somatic *MEN1* mutations.

How menin blocks MAPK-driven proliferation in endocrine cells remains unclear. Menin localizes to the nucleus and chromatin-modifying complexes including MLL and can regulate gene expression (52, 53), but it has been shown to block cell proliferation by multiple mechanisms, including modulating both

transcriptional regulators and cell signaling pathway components through direct protein-protein interactions (52–54). Identifying the unique targets of the MAPK pathway in menin WT and mutant endocrine cells may provide insight into the unique sensitivity of endocrine cells to loss of menin.

In addition to providing new insights into endocrine growth and tumorigenesis, the model in Figure 5J also suggests potential therapeutic targets for diabetes. Diabetes treatment has the opposite objective of antineoplastic therapies, that of enhancing proliferation to regenerate β cell mass, which is a major and currently unmet goal in the treatment of both type 1 and type 2 diabetes. Therefore, appropriate combinations of inhibition and activation of specific K-RAS pathway components may represent a rational strategy for inducing β cell proliferation and restoration for people with diabetes.

In conclusion, our study provides fresh insight into the unique pathways that regulate endocrine cell growth and presents what we believe to be a novel mechanism for the cell type–specific control of K-RAS function.

Methods

Animals. Mice were housed on a 12-hour light/12-hour dark cycle in controlled-climate rooms (21.5–22.5°C). The *Kras*^{G12D} (12), *Men1*$^{+/fl}$ (25), *Rassf1a*$^{+/-}$ (21), *R26*^{mTmG} (55), *Pdx1-Cre* (56), and *Ins2-Cre* (57) transgenic mouse lines were maintained and genotyped as previously described. Noon of the day on which a vaginal plug was detected was considered E0.5.

Glucose tolerance tests. A glucose tolerance test (GTT) was performed on 10-week-old male mice that had been placed on a high-fat diet (Research Diets) for 6 weeks beginning at 4 weeks of age. All mice were fasted overnight and placed in fresh cages to ensure that no food was available on the cage floor. The following morning, each mouse was intraperitoneally injected with glucose dissolved in water (2 g/kg body weight). Glucose measurements were taken from tail blood at the indicated times (see Supplemental Figure 3) using a FreeStyle Freedom Lite glucose meter (Abbott Laboratories).

Pancreatic histology. Mice were euthanized by carbon dioxide asphyxiation, and tissues were isolated by dissection using a dissecting stereoscope. Tissues were then fixed in 4% paraformaldehyde (PFA) at 4°C for 2 hours. Tissues were sectioned at a thickness of 10 microns on a cryostat and mounted on Superfrost Plus glass slides (Fisher Scientific). Sections were postfixed for 10 minutes and then incubated with primary antibodies against insulin (Dako); glucagon (Dako and EMD Millipore); p-H3 (Ser10) (EMD Millipore); B-RAF (Sigma-Aldrich); RASSF1A (Sigma-Aldrich); ERK1/2 (Abcam and generated by M.H. Cobb); p-ERK1/2 (Thr202/Tyr204) (Cell Signaling Technology and Sigma-Aldrich); chromogranin A (Thermo Fisher Scientific,); menin (Abcam); Ki-67 (Abcam), GFP (Aves Labs); and prolactin (R&D Systems). p-RASSF1A (Ser131) was a gift of Eric O'Neill (Department of Oncology, University of Oxford, Oxford, United Kingdom) (17). Antibodies were diluted in PBS with 0.5% Triton X-100 (PBTX) (Sigma-Aldrich) and 5% donkey serum (Jackson ImmunoResearch Laboratories) and incubated with slides for 2 hours at room temperature or overnight at 4°C in a humidified chamber, followed by 3 washes in cold PBS. Slides were then incubated with fluorescent secondary antibodies (Invitrogen) that had been diluted in PBTX with 5% donkey serum at 1:300 for 1 hour at room temperature or overnight at 4°C in a humidified chamber, followed by 3 washes in cold PBS. Slides were then stained for DNA using either Topro3 (Invitrogen), DAPI (Invitrogen), or Hoechst 33342 (Invitrogen) at a dilution of 1:10,000 in all cases. Slides were then coverslipped with VECTASHIELD HardSet Mounting Medium (Vector Laboratories). Images were collected using a Zeiss LSM 510 confocal microscope.

For measurement of pancreatic α and β cell area, every fifth pancreatic section was examined on a Zeiss LSM 510 confocal microscope using a ×10 objective. The area of fluorescently stained β cells was quantified using ImageJ software (NIH). Pancreas weight was measured on a scale.

Parathyroid size measurement. The product of the maximum length and width from the largest parathyroid tissue cross section was used as a measurement for size. The length axis and width axis were orthogonal within the cross-sectional plane.

Whole-mount analysis of embryonic pancreata. Pregnant female mice were euthanized 13 days postcoitum by carbon dioxide asphyxiation, and embryos were harvested by dissection using a dissecting stereoscope. Tissues were then fixed in 4% PFA at 4°C overnight and placed in 100% methanol. Next, tissues were treated with 5% hydrogen peroxide for 5 hours and then washed with methanol 3 times and rehydrated into PBS containing 0.1% Tween-20 (Sigma-Aldrich). Tissues were then incubated with primary antibodies against neurogenin 3 (German laboratory; ref. 14), insulin (Dako), glucagon (Dako), and E-cadherin (Invitrogen), which had been diluted in PBTX with 5% donkey serum overnight at 4°C, followed by 3 washes in cold PBTX. For neurogenin 3, insulin, and glucagon staining, tissues were then incubated with fluorescent secondary antibodies (Invitrogen) that had been diluted in PBTX with 5% donkey serum at 1:300 overnight at 4°C, followed by 3 washes in cold PBTX. For E-cadherin, tissues were instead incubated with a biotinylated rabbit anti-rat antibody (Vector Laboratories) overnight at 4°C, followed by 3 washes in cold PBTX. Tissues were then incubated with a streptavidin-conjugated horseradish peroxidase from the VECTASTAIN Elite ABC kit (Vector Laboratories) for 2 hours at room temperature, followed by 3 washes in cold PBTX. Tissues were then incubated with fluorescent tyramide (PerkinElmer) for 30 minutes at room temperature, followed by 3 washes in cold PBTX. For imaging, stained tissues were placed in 100% methanol and cleared using a 1:2 mixture of benzyl alcohol/benzyl benzoate and placed into a custom-made glass chamber. A *z* series through the intact embryonic pancreas was collected on a Zeiss LSM 510 confocal microscope using a ×10 objective. The area of fluorescent staining throughout the sample was quantified using ImageJ software. Measurements were normalized using the average value from control samples.

Gene expression studies. Gene expression from adult β cells (Supplemental Figure 9) was derived from reanalysis of the data from ref. 16.

Islet culture and proliferation assessment. Mouse and human pancreatic islets were isolated by collagenase digestion and were then handpicked as previously described (58). Mouse islets were obtained from P5 neonates and 12-week-old male mice. Human islets were obtained by the UCSF Diabetes Research Center Islet Core Laboratory from deceased donors (donor 1: 22-year-old male; donor 2: 23-year-old female; donor 3: 28-year-old male; donor 4: 42-year-old male; donor 5: 48-year-old female; donor 6: 55-year-old male). For proliferation studies, islets were cultured for 5 days in RPMI-1640 media and treated with FTI-GGTI inhibitors (10 μM and 20 μM, respectively) (Sigma-Aldrich); 10 μM PD0325901 (Sigma-Aldrich); 10 μM GSK1120212 (Selleck Chemicals);

90 nM exendin-4 (Sigma-Aldrich); 1 μM MI-2 (XcessBio); or DMSO (Sigma-Aldrich). Medium with these additives was freshly made and replaced daily. On day 5 of treatment, islets were incubated with 10 μM EdU (Invitrogen) (mouse islets for 16 hours; human islets for 48 hours) and then fixed in 4% PFA for 2 hours. Fixed islets were washed 3 times with PBS and then incubated with primary antibodies raised against NKX6.1 (Sigma-Aldrich) in PBTX with 5% donkey serum overnight at 4°C, followed by 3 washes in cold PBTX. Islets were then incubated with fluorescent secondary antibodies (Invitrogen) that had been diluted in PBTX with 5% donkey serum at 1:300 overnight, followed by 3 washes in cold PBS. Islets were then stained for DNA using either Topro3, DAPI, or Hoechst 33342, at a dilution of 1:10,000 in all cases. After staining, replicating cells were labeled with the Click-iT EdU Alexa Fluor Imaging Kit (Invitrogen). Islets were placed in VECTASHIELD and imaged using a Leica SP5 confocal laser scanning microscope. ImageJ software was used to count NKX6.1/EdU–double-positive nuclei. The relative percentage of proliferating β cells was calculated by dividing the number of nuclei costaining EdU and NKX6.1 by the total number of $NKX6.1^+$ nuclei and then normalized using control values. For immunoblots, islets were cultured overnight (PD0325901) or overnight and then for 30 minutes with fresh inhibitors (FTI-GGTI), before harvesting.

MIN6 insulinoma cell culture. MIN6 insulinoma cells (59) were maintained in DMEM supplemented with 15% FBS, 100 units/ml penicillin, 100 g/ml streptomycin, and 71.5 μM β-mercaptoethanol. A MIN6 subclone with low menin expression was used for this study. For proliferation studies, MIN6 insulinoma cells were plated on Permanox 8-well chamber slides (Electron Microscopy Sciences) on day 0, transfected on day 1, treated on days 2 and 3, and then fixed in 4% PFA for 1 hour on day 4. Transient transfection of MIN6 insulinoma cells was performed using Lipofectamine 2000 reagent (Invitrogen).

Immunoblotting. Immunoblotting was performed using standard procedures. Briefly, cells or islets were lysed in buffer containing 50 mM HEPES (pH 7.5), 150 mM NaCl, 1% Triton X-100, and Halt Protease Inhibitor Cocktail (Pierce Biotechnology). Lysates containing 40 μg of protein, as determined by Bradford Reagent (Bio-Rad), were resolved by SDS-PAGE and transferred to nitrocellulose or PVDF membranes (Bio-Rad). Membranes were blocked with 5% nonfat milk and/or 5% fraction-V BSA (Sigma-Aldrich) in Tris-buffered saline containing 0.1% Tween-20 (TBST). Membranes were incubated with primary antibodies overnight at 4°C. The following primary antibodies were used: p-ERK1/2 (Sigma-Aldrich and Cell Signaling Technology) and ERK1/2 (Abcam and as described in ref. 60). RASSF1 (Sigma-Aldrich) and p-RASSF1A (Ser131) (17) antibodies were preabsorbed using pancreatic tissue powder derived from neonatal or adult *Rassf1a*$^{-/-}$ mice. Membranes were washed with TBST and incubated with the following secondary antibodies: donkey anti-rabbit IRDye 680RD (LI-COR Biosciences); donkey anti-mouse IRDye 800CW (LI-COR Biosciences); donkey anti-rabbit HRP (Cell Signaling Technology); and donkey anti-mouse HRP (Cell Signaling Technology). For multiple detection, membranes were stripped using stripping buffer (Thermo Fisher Scientific). Membranes were imaged using either the LI-COR Odyssey Infrared imaging system or x-ray film and a flat-bed scanner.

Generation of menin$^+$ *iresGFP plasmid*. The plasmid pMenin$^+$iresGFP was generated by inserting coding in tandem sequences for human menin (Addgene; ref. 61), an internal ribosomal entry site (ires), and GFP into the pCAGG mammalian expression vector (62).

Statistics. All data points were compared using a 2-tailed Student's *t* test, and a *P* value of less than 0.05 was considered statistically significant.

Study approval. All procedures were approved by the IACUC of the UCSF and were conducted in accordance with regulations of the UCSF, which gave ethical approval for these studies.

Acknowledgments

We thank W. Rutter, G. Grodsky, M. McMahon, and members of the German, Kajimura, Martin, and Hebrok laboratories for helpful discussions; F. Salim and A. Stewart for assistance with human islet experiments; Z. Pappalardo and G. Szot for technical advice and assistance; and P. Walter, F. Collins, M. McMahon, G. Hamilton, T. Jacks, D. Melton, S. Luo, M. Magnusen, S. Tommasi, and G. Pfeifer for sharing equipment and reagents. This work was supported by grants from the Larry L. Hillblom Foundation (2007/1B, to M.S. German), the Juvenile Diabetes Research Foundation (16-2007-428, to M.S. German; 3-2007-721, to T. Miyatsuka; 3-2011-166, to C.E. Chamberlain), Cancer Research UK (A19277, to E. O'Neill), and the NIH (R01 DK55310, to M.H. Cobb; R01 DK021344, U01 DK089541, and P30 DK63720, to M.S. German).

Address correspondence to: Michael S. German, Regeneration Medicine Building, 35 Medical Center Way, Box 0669, San Francisco, California 94143, USA. Phone: 415.476.9262; E-mail: mgerman@diabetes.ucsf.edu.

1. Malumbres M, Barbacid M. RAS oncogenes: the first 30 years. *Nat Rev Cancer*. 2003;3(6):459–465.
2. Pylayeva-Gupta Y, Grabocka E, Bar-Sagi D. RAS oncogenes: weaving a tumorigenic web. *Nat Rev Cancer*. 2011;11(11):761–774.
3. Karnoub AE, Weinberg RA. Ras oncogenes: split personalities. *Nat Rev Mol Cell Biol*. 2008;9(7):517–531.
4. Gidekel Friedlander SY, et al. Context-dependent transformation of adult pancreatic cells by oncogenic K-Ras. *Cancer Cell*. 2009;16(5):379–389.
5. Jones S, et al. Core signaling pathways in human pancreatic cancers revealed by global genomic analyses. *Science*. 2008;321(5897):1801–1806.
6. Jiao Y, et al. DAXX/ATRX, MEN1, and mTOR pathway genes are frequently altered in pancreatic neuroendocrine tumors. *Science*. 2011;331(6021):1199–1203.
7. House MG, et al. Aberrant hypermethylation of tumor suppressor genes in pancreatic endocrine neoplasms. *Ann Surg*. 2003;238(3):423–431.
8. Dammann R, et al. Epigenetic inactivation of the Ras-association domain family 1 (RASSF1A) gene and its function in human carcinogenesis. *Histol Histopathol*. 2003;18(2):665–677.
9. Dammann R, et al. Frequent RASSF1A promoter hypermethylation and K-ras mutations in pancreatic carcinoma. *Oncogene*. 2003;22(24):3806–3812.
10. van der Weyden L, Adams DJ. The Ras-association domain family (RASSF) members and their role in human tumourigenesis. *Biochim Biophys Acta*. 2007;1776(1):58–85.
11. Chandrasekharappa SC, et al. Positional cloning of the gene for multiple endocrine neoplasia-type 1. *Science*. 1997;276(5311):404–407.
12. Tuveson DA, et al. Endogenous oncogenic K-ras(G12D) stimulates proliferation and widespread neoplastic and developmental defects. *Cancer Cell*. 2004;5(4):375–387.
13. Finegood DT, Scaglia L, Bonner-Weir S. Dynamics of β-cell mass in the growing rat pancreas. Estimation with a simple mathematical model. *Diabetes*. 1995;44(3):249–256.
14. Schwitzgebel VM, et al. Expression of neurogenin3 reveals an islet cell precursor population in the pancreas. *Development*. 2000;127(16):3533–3542.
15. Shields JM, Pruitt K, McFall A, Shaub A, Der CJ. Understanding Ras: 'it ain't over 'til it's over'. *Trends Cell Biol*. 2000;10(4):147–154.
16. Ku GM, et al. Research resource: RNA-Seq

reveals unique features of the pancreatic β-cell transcriptome. *Mol Endocrinol*. 2012;26(10):1783–1792.
17. Hamilton G, Yee KS, Scrace S, O'Neill E. ATM regulates a RASSF1A-dependent DNA damage response. *Curr Biol*. 2009;19(23):2020–2025.
18. Wan PT, et al. Mechanism of activation of the RAF-ERK signaling pathway by oncogenic mutations of B-RAF. *Cell*. 2004;116(6):855–867.
19. Ahearn IM, Haigis K, Bar-Sagi D, Philips MR. Regulating the regulator: post-translational modification of RAS. *Nat Rev Mol Cell Biol*. 2012;13(1):39–51.
20. Sebolt-Leopold JS, Herrera R. Targeting the mitogen-activated protein kinase cascade to treat cancer. *Nat Rev Cancer*. 2004;4(12):937–947.
21. Tommasi S, et al. Tumor susceptibility of Rassf1a knockout mice. *Cancer Res*. 2005;65(1):92–98.
22. Crabtree JS, et al. A mouse model of multiple endocrine neoplasia, type 1, develops multiple endocrine tumors. *Proc Natl Acad Sci U S A*. 2001;98(3):1118–1123.
23. Karnik SK, et al. Menin regulates pancreatic islet growth by promoting histone methylation and expression of genes encoding p27Kip1 and p18INK4c. *Proc Natl Acad Sci U S A*. 2005;102(41):14659–14664.
24. Schnepp RW, et al. Mutation of tumor suppressor gene Men1 acutely enhances proliferation of pancreatic islet cells. *Cancer Res*. 2006;66(11):5707–5715.
25. Libutti SK, et al. Parathyroid gland-specific deletion of the mouse Men1 gene results in parathyroid neoplasia and hypercalcemic hyperparathyroidism. *Cancer Res*. 2003;63(22):8022–8028.
26. Gallo A, et al. Menin uncouples Elk-1, JunD and c-Jun phosphorylation from MAP kinase activation. *Oncogene*. 2002;21(42):6434–6445.
27. Luo J, Solimini NL, Elledge SJ. Principles of cancer therapy: oncogene and non-oncogene addiction. *Cell*. 2009;136(5):823–837.
28. Gilmartin AG, et al. GSK1120212 (JTP-74057) is an inhibitor of MEK activity and activation with favorable pharmacokinetic properties for sustained in vivo pathway inhibition. *Clin Cancer Res*. 2011;17(5):989–1000.
29. Arnette D, et al. Regulation of ERK1 and ERK2 by glucose and peptide hormones in pancreatic beta cells. *J Biol Chem*. 2003;278(35):32517–32525.
30. Grembecka J, et al. Menin-MLL inhibitors reverse oncogenic activity of MLL fusion proteins in leukemia. *Nat Chem Biol*. 2012;8(3):277–284.
31. Serrano M, Lin AW, McCurrach ME, Beach D, Lowe SW. Oncogenic ras provokes premature cell senescence associated with accumulation of p53 and p16INK4a. *Cell*. 1997;88(5):593–602.
32. Zhang Z, et al. Wildtype Kras2 can inhibit lung carcinogenesis in mice. *Nat Genet*. 2001;29(1):25–33.
33. Almoguera C, Shibata D, Forrester K, Martin J, Arnheim N, Perucho M. Most human carcinomas of the exocrine pancreas contain mutant c-K-ras genes. *Cell*. 1988;53(4):549–554.
34. Liu L, et al. Epigenetic alterations in neuroendocrine tumors: methylation of RAS-association domain family 1, isoform A and p16 genes are associated with metastasis. *Mod Pathol*. 2005;18(12):1632–1640.
35. Pizzi S, et al. RASSF1A promoter methylation and 3p21.3 loss of heterozygosity are features of foregut, but not midgut and hindgut, malignant endocrine tumours. *J Pathol*. 2005;206(4):409–416.
36. Malpeli G, et al. Methylation-associated down-regulation of RASSF1A and up-regulation of RASSF1C in pancreatic endocrine tumors. *BMC Cancer*. 2011;11:351.
37. Ahmed-Choudhury J, et al. Transcriptional regulation of cyclin A2 by RASSF1A through the enhanced binding of p120E4F to the cyclin A2 promoter. *Cancer Res*. 2005;65(7):2690–2697.
38. Fenton SL, et al. Identification of the E1A-regulated transcription factor p120 E4F as an interacting partner of the RASSF1A candidate tumor suppressor gene. *Cancer Res*. 2004;64(1):102–107.
39. Agathanggelou A, et al. Identification of novel gene expression targets for the Ras association domain family 1 (RASSF1A) tumor suppressor gene in non-small cell lung cancer and neuroblastoma. *Cancer Res*. 2003;63(17):5344–5351.
40. Shivakumar L, Minna J, Sakamaki T, Pestell R, White MA. The RASSF1A tumor suppressor blocks cell cycle progression and inhibits cyclin D1 accumulation. *Mol Cell Biol*. 2002;22(12):4309–4318.
41. Whang YM, Kim YH, Kim JS, Yoo YD. RASSF1A suppresses the c-Jun-NH2-kinase pathway and inhibits cell cycle progression. *Cancer Res*. 2005;65(9):3682–3690.
42. Rong R, Jin W, Zhang J, Sheikh MS, Huang Y. Tumor suppressor RASSF1A is a microtubule-binding protein that stabilizes microtubules and induces G2/M arrest. *Oncogene*. 2004;23(50):8216–8230.
43. Song MS, et al. The tumour suppressor RASSF1A regulates mitosis by inhibiting the APC-Cdc20 complex. *Nat Cell Biol*. 2004;6(2):129–137.
44. Ortiz-Vega S, et al. The putative tumor suppressor RASSF1A homodimerizes and heterodimerizes with the Ras-GTP binding protein Nore1. *Oncogene*. 2002;21(9):1381–1390.
45. Yoshimoto K, et al. ras mutations in endocrine tumors: mutation detection by polymerase chain reaction-single strand conformation polymorphism. *Jpn J Cancer Res*. 1992;83(10):1057–1062.
46. Herman V, Drazin NZ, Gonsky R, Melmed S. Molecular screening of pituitary adenomas for gene mutations and rearrangements. *J Clin Endocrinol Metab*. 1993;77(1):50–55.
47. Cai WY, et al. ras mutations in human prolactinomas and pituitary carcinomas. *J Clin Endocrinol Metab*. 1994;78(1):89–93.
48. Karga HJ, Alexander JM, Hedley-Whyte ET, Klibanski A, Jameson JL. Ras mutations in human pituitary tumors. *J Clin Endocrinol Metab*. 1992;74(4):914–919.
49. Juhlin CC, et al. Frequent promoter hypermethylation of the APC and RASSF1A tumour suppressors in parathyroid tumours. *PLoS One*. 2010;5(3):e9472.
50. Qian ZR, et al. Inactivation of RASSF1A tumor suppressor gene by aberrant promoter hypermethylation in human pituitary adenomas. *Lab Invest*. 2005;85(4):464–473.
51. Agarwal SK, et al. Germline mutations of the MEN1 gene in familial multiple endocrine neoplasia type 1 and related states. *Hum Mol Genet*. 1997;6(7):1169–1175.
52. Balogh K, Patocs A, Hunyady L, Racz K. Menin dynamics and functional insight: take your partners. *Mol Cell Endocrinol*. 2010;326(1):80–84.
53. Agarwal SK, et al. Menin molecular interactions: insights into normal functions and tumorigenesis. *Horm Metab Res*. 2005;37(6):369–374.
54. Wu Y, et al. Interplay between menin and K-Ras in regulating lung adenocarcinoma. *J Biol Chem*. 2012;287(47):40003–40011.
55. Muzumdar MD, Tasic B, Miyamichi K, Li L, Luo L. A global double-fluorescent Cre reporter mouse. *Genesis*. 2007;45(9):593–605.
56. Gu G, Dubauskaite J, Melton DA. Direct evidence for the pancreatic lineage: NGN3$^+$ cells are islet progenitors and are distinct from duct progenitors. *Development*. 2002;129(10):2447–2457.
57. Postic C, et al. Dual roles for glucokinase in glucose homeostasis as determined by liver and pancreatic β cell-specific gene knock-outs using Cre recombinase. *J Biol Chem*. 1999;274(1):305–315.
58. Szot GL, Koudria P, Bluestone JA. Murine pancreatic islet isolation. *J Vis Exp*. 2007;(7):255.
59. Miyazaki J, et al. Establishment of a pancreatic β cell line that retains glucose-inducible insulin secretion: special reference to expression of glucose transporter isoforms. *Endocrinology*. 1990;127(1):126–132.
60. Boulton TG, Cobb MH. Identification of multiple extracellular signal-regulated kinases (ERKs) with antipeptide antibodies. *Cell Regul*. 1991;2(5):357–371.
61. Hughes CM, et al. Menin associates with a trithorax family histone methyltransferase complex and with the hoxc8 locus. *Mol Cell*. 2004;13(4):587–597.
62. Niwa H, Yamamura K, Miyazaki J. Efficient selection for high-expression transfectants with a novel eukaryotic vector. *Gene*. 1991;108(2):193–199.